

Article

Study on Mechanical Properties of Surrounding Rock and Combined Stress of Composite Lining in the Diversion Tunnel

Yan Jiang ^{1,2}, Wenlong Wang ¹, Guanghua Yang ², Jinchao Yue ¹ and Yibin Huang ^{1,*}¹ Yellow River Laboratory, Zhengzhou University, Zhengzhou 450001, China² Geotechnical Engineering Research Institute, Guangdong Research Institute of Water Resources and Hydropower, Guangzhou 510610, China

* Correspondence: huangyb@zzu.edu.cn; Tel.: +86-188-0371-2901

Abstract: To determine the mechanical properties of the rock mass in the Nansha Branch, three in-situ tests (on-site pressure plate, borehole TV and acoustic wave, and borehole deformation methods) were carried out. Based on the deformation characteristics of the rock mass, the finite element numerical method is used to study the combined stress of the composite lining in the diversion tunnel. The results demonstrate that the deformation modulus values are similar by comparing them to tests of the pressure plate and borehole deformation method. It shows the accuracy and reliability of the deformation modulus obtained by the borehole deformation method. In addition, the deformation modulus of the borehole deformation method and wave velocity were fitted to obtain a power function relationship. The deformation modulus of the pelitic siltstones was estimated. After the Nansha Branch tunnel is filled with water, the maximum principal stress of the pipe piece is 1.953 Mpa in tensile stress, located at the outside of the waist on both sides of the pipe piece. The maximum principal stress of the reinforced concrete lining is 5.407 Mpa, located at the top and bottom inside. The maximum principal stresses have exceeded the standard tensile strength of both the pipe piece and reinforced concrete and are vulnerable to cracking. Special attention should be paid to the deformation of the above parts with regard to long-term operation.

Keywords: surrounding rock deformation; in situ test; composite lining; diversion tunnel; combined stress



Citation: Jiang, Y.; Wang, W.; Yang, G.; Yue, J.; Huang, Y. Study on Mechanical Properties of Surrounding Rock and Combined Stress of Composite Lining in the Diversion Tunnel. *Appl. Sci.* **2023**, *13*, 3849. <https://doi.org/10.3390/app13063849>

Academic Editor: Daniel Dias

Received: 20 February 2023

Revised: 13 March 2023

Accepted: 16 March 2023

Published: 17 March 2023



Copyright: © 2023 by the authors. Licensee MDPI, Basel, Switzerland. This article is an open access article distributed under the terms and conditions of the Creative Commons Attribution (CC BY) license (<https://creativecommons.org/licenses/by/4.0/>).

1. Introduction

The distribution of water resources is restricted by geography, topography, precipitation, and other factors. To meet people's demands for habitation and productivity, interregional and interbasin water transfer have developed into an engineering strategy for the optimal allocation of water resources. The diversion tunnel is a crucial component of the water conservation project. It is often located in complex surrounding geological environments such as fault development, aquifers, and more permeable layers. Its stability is directly influenced by the deformation characteristics of the surrounding rock [1,2]. The deformation characteristics of rocks are frequently obtained by laboratory and in situ experiments [3–5] for the project's safety and economics, providing an essential engineering geological foundation.

The deformation mechanism of the rock mass has been revealed according to previous studies. Han and He et al. [6,7] conducted uniaxial and triaxial tests on rocks with different water contents to obtain the deformation mechanical properties and damage modes of the rocks under different loading paths. Meng and Vaneghi et al. [8–10] revealed the laws of the influence under circumferential pressure and cyclic loading on the deformation and damage mechanisms of rocks through triaxial and uniaxial cyclic loading tests. Sabitova et al. [11] found that rock viscosity values correlate well with failure properties through multistage triaxial experiments. Whereas the deformation properties of rocks under various situations were explored in the indoor testing, the impact of the rock field environment

on the deformation characteristics was disregarded. Many fractures, joints, and other geological formations are distributed in the rock mass [12,13]. As a result of these weak zones, the rock mass's overall deformation characteristics are weaker than the rock mass itself. In situ tests are required to reflect such deformation characteristics. Singh and Hua et al. [14,15] estimated the deformation modulus of rock masses in different places by pressure in situ testing, respectively. Radovanovic et al. [16] developed a statistical model correlating the deformation modulus with the measured values of longitudinal wave velocity and pressure in the rock mass based on multiple linear regression and artificial neural networks using the results of in situ tests in the field. Asem [17] proposed a model for predicting the deformation modulus and unconfined compressive strength based on the penetration rate using in situ tests from 21 weak rock sites in Illinois, United States. Although the above researchers conducted in situ tests, they did not compare different in situ tests to estimate the deformation modulus. In future studies, the relationship between different testing means can be found by comparing different in situ tests and selecting the most applicable rock parameters for the project.

The rock parameters are the basis for the design model of the diversion tunnel. Currently, most diversion tunnels' inner and outer liners with immense internal water pressure support themselves independently in a costly, unscientific, and conservative safety mode. Due to the immature research on the combined stress mode and the lack of corresponding engineering design experience, it is rarely applied in engineering. A more scientific model of the combined stress mode of the inner and outer linings and the surrounding rock is needed. Naggar et al. [18] presented flexible solutions for displacement and stress. Mason and Abelman [19] presented an elastic analytical solution for double-layered liners subjected to uniform shear stresses at infinity. Li et al. [20] suggested a streamlined algorithm to precisely determine the stress distribution in composite lining after taking into account the impact of internal water pressure and adjacent rock on the composite lining. Gu et al. [21] analyzed the viscoelastic-plastic properties of the surrounding rock using the unified strength theory and derived equations to calculate the stress–strain relationship of the composite lining during the creep of the surrounding rock. Cao et al. [22] discussed the variation law of crack width for different reinforcement rates, reinforcement location, lining thickness, surrounding rock type, tunnel radius, and concrete strength, considering the restraint of reinforcement and the combined stress of the rock and lining. Although there are quite a lot of studies on the composite lining, there are fewer studies of combined stress on the composite lining, which will be the most challenging and innovative, as well as the most valuable research topic.

In this paper, relying on the Pearl River Delta water resources allocation project, the power function relationship between rock deformation modulus and wave velocity was obtained by analyzing and comparing the results of three in situ tests. Parameters that can be applied to the project are selected. The deformation characteristics of the surrounding rock were revealed. Based on the deformation of the surrounding rock and the dynamic evolution of permeability and porosity, the deformation characteristics of pipe pieces and reinforced concrete are analyzed by using ABAQUS secondary development under the combined stress model of the composite lining.

2. Project and Geology Overview

The layout of the water resources allocation project in Pearl River Delta is shown in Figure 1. The Nansha Branch line, which has a flow range of 5–13 m³/s, uses gravity self-flow water transmission and is designed to supply 13 m³/s. The shield tunnel length is 7.4 km and uses a single-line shield water transmission tunnel scheme. The concrete shield segment with inner and outer linings withstand internal and exterior pressure, respectively. The shield tunnel diameter is 4.1 m. The pipe piece thickness is 0.3 m and the inner diameter is 3.5 m. The lining C35 reinforced concrete thickness is 0.35 m. The tunnel water transmission inner diameter is 2.8 m. Moreover, there is a 1.2 mm waterproofing membrane put in between the pipe piece and the reinforced concrete. The composite liner

must withstand a maximum internal pressure of 0.76 MPa under the conditions of the water transmission pressure of 0.7 MPa and surge pressure of 0.06 MPa.

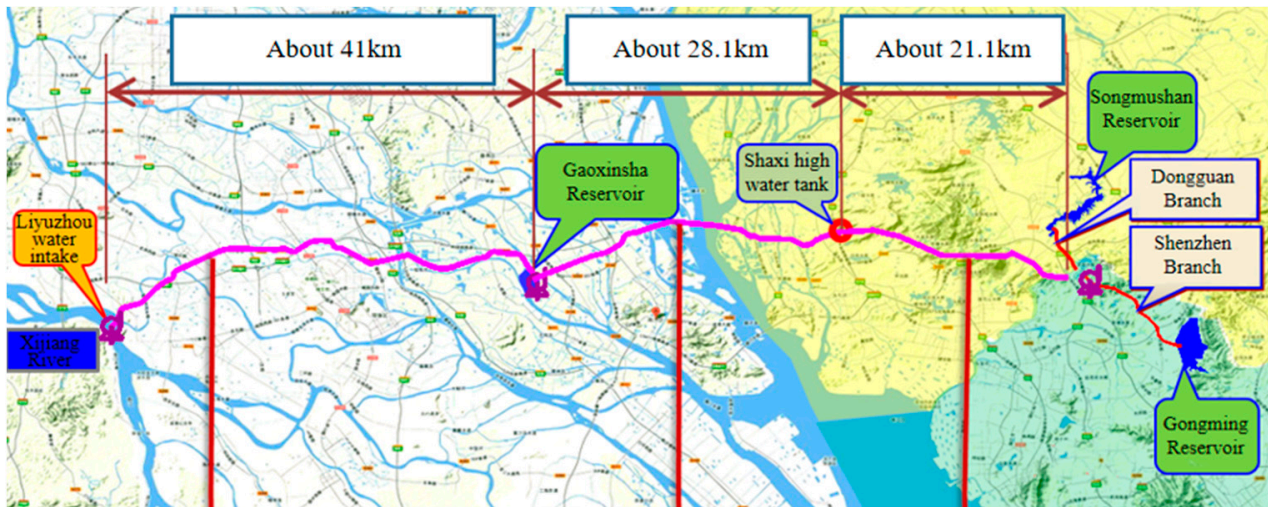


Figure 1. Layout sketch of water resources allocation project.

The Nansha Branch is dominated by the delta plain landform, with the development of rivers and waterways, sporadic hill remnants, and generally flat topography. The bedrock from top to bottom is composed of artificial fill, silt, silty clay, medium and coarse gravelly sand, and weakly weathered pelitic siltstone. The pelitic siltstones are mainly distributed in the depositional Tertiary Lower Xinzhuangcun Formation (E1x) and the Cretaceous Lower Baizhishan Formation (K1b). Due to the influence of composition and water on the weathering rate, pelitic siltstones with different degrees of weathering are produced. The object of this test study is the weakly weathered pelitic siltstone of the Lower Tertiary Xinzhuang Village Formation (E1x) and the Tertiary rock production EW/N10°~20°.

During the wet season, groundwater recharge primarily occurs through atmospheric precipitation, rivers, and channels. During the dry season, groundwater recharge to rivers is controlled by tides. Surface water and groundwater complement each other's drainage systems. The 50-year exceedance probability of 10% in the area is 0.10 g, and the corresponding essential earthquake intensity is VII. The characteristic period of the basic ground motion response spectrum is 0.35 s. The classification of regional tectonic stability is favorable.

3. Test of the Surrounding Rock

3.1. In Situ Rock Deformation Test of the Pressure Plate

The deformation test of the pressure plate at the project site was carried out. The deformation modulus of surrounding rock under the water transfer and maximum test pressure is analyzed. A total of six tests were set up on the project site, with the test points placed on the side wall of a test pit. The location layout of the test site and the pressure plate test loading are shown in Figure 2. #1 to #6 represent test locations of the six pressure plate, respectively. The test pit's long side forms a 105° angle with the shield tunneling direction; its top elevation is roughly 25.5 m; its depth is approximately 2.5 m. The elevation of the test center point is about 27.2 m. Its elevation outside the shaft is nearly 3.7 m. The diameter circular rigid pressure plate of 0.30 m was imposed by using a 20 t jack. The maximum test pressure of 2.1 MPa is about three times the design pressure.

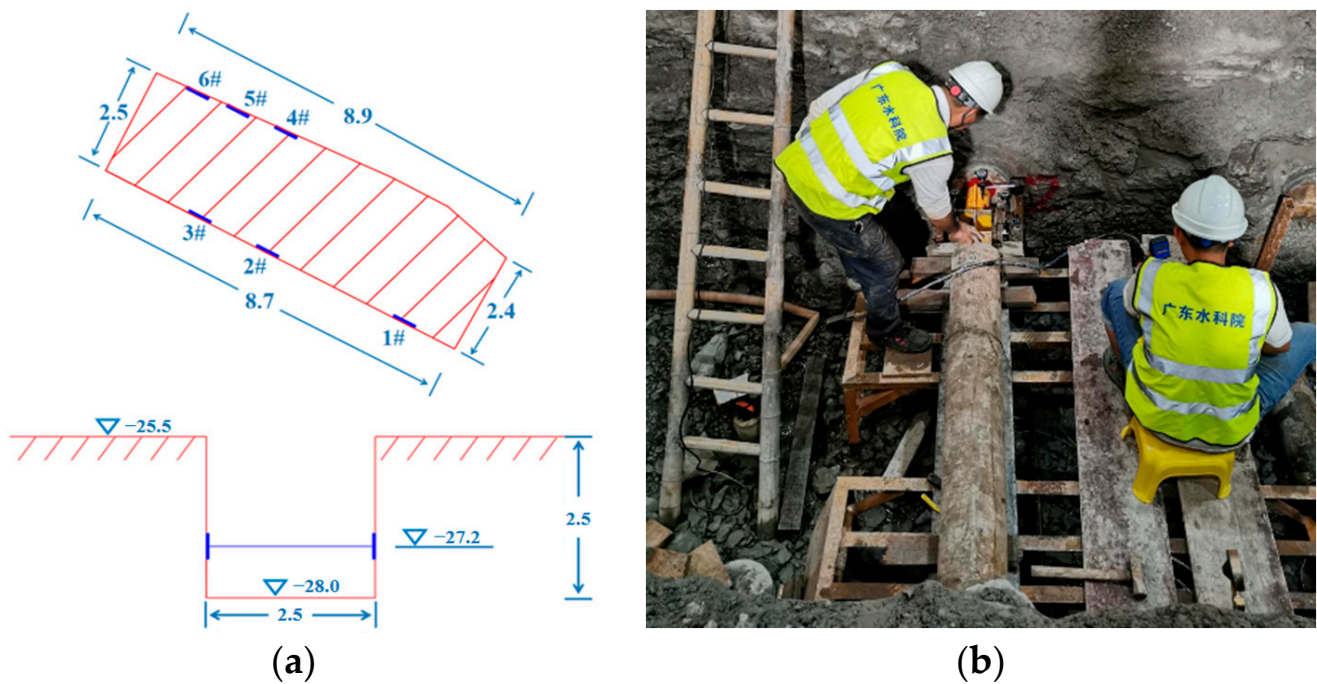


Figure 2. In situ pressure plate test. (a) Site layout. (b) Field loading test.

By measuring the surface deformation of the rock mass using a pressure plate test, the deformation modulus was calculated. And the deformation modulus of the borehole deformation test was compared. The test pit was located in a weakly weathered pelitic siltstone layer. The lithology of the six test points is relatively complete; weakly weathered pelitic siltstone without obvious fracture development. Under two stress levels of water delivery pressure of 0.7 MPa and a maximum test pressure of 2.1 MPa, the secant and fitting methods were used to compare and analyze the deformation modulus. The calculated deformation modulus at the highest point of the test pressure is shown in Table 1.

Table 1. Deformation modulus of each test point.

Stress Level (Mpa)	Calculation Method	Test Point (Gpa)						Average (Gpa)
		1	2	3	4	5	6	Es
2.1	Secant line	1.30	4.11	2.27	2.10	9.63	8.07	4.58
2.1	Fitting	1.31	4.33	2.38	2.02	9.60	8.52	4.69
0.7	Fitting	1.16	5.53	2.68	1.71	8.84	8.33	4.71

The results indicate that the fitting and the secant method are nearly identical to each other. According to statistical fitting method data, the deformation modulus of each test point under stress close to the water transmission pressure of the engineering design is 1.16~8.84 GPa, and the average value is 4.71 GPa. The deformation modulus calculated by the maximum test pressure is 1.31~9.60 GPa, and the average value is 4.69 GPa. The fitted curve of test point No. six at the highest point of test pressure is shown in Figure 3.

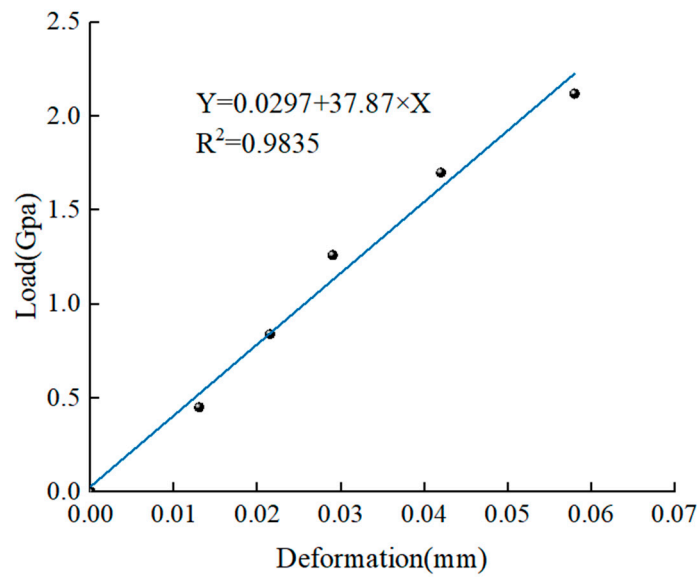


Figure 3. The fitting curve of the pressure plate test at the No. six test point.

3.2. On-Site Borehole TV and Acoustic Wave Test

Six evenly spaced boreholes, each with a single hole depth of approximately 38 m, surround the working well (the burial depth of the diversion tunnel is about 30 m). The wave speed test is carried out by the single-hole method, with excitation in the hole. The probes from top to bottom are the transmitter, geophone 1, and geophone 2. The wave from the vibration source is received by the geophone in the hole. The time for the wave to travel from geophone 1 to geophone 2 is calculated, as shown in Figure 4. The wave speed can be found as follows:

$$V = L/t \tag{1}$$

where V is the wave velocity (m/s), L is the distance between two sensors (m), t is the time between two sensors (s).

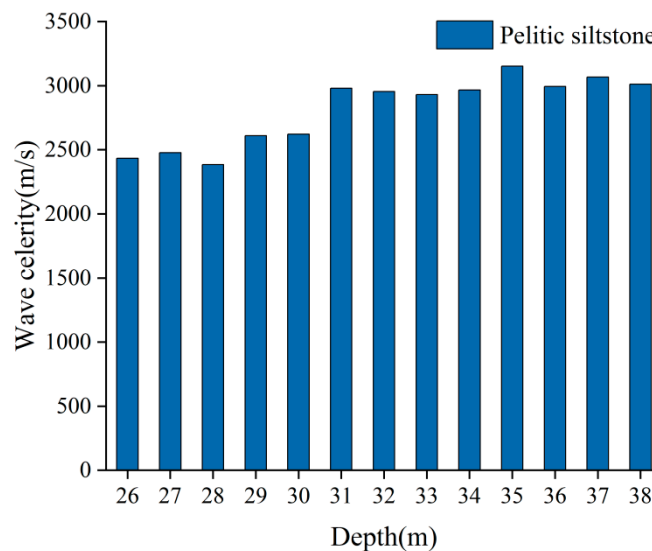


Figure 4. Borehole acoustic wave velocity at each depth.

Each borehole bedrock section was subjected to in situ borehole television and acoustic wave tests. The development and integrity of the surrounding rock bedding are obtained through borehole television. The horizontal bedding of the surrounding rock is developed, and the integrity of the surrounding rock in the local hole section is poor according to the

borehole television. The number of steep dip fractures is limited, but the width is large and there is a corrosion phenomenon. According to the acoustic wave test, the average wave speed of the lightly weathered muddy siltstone was 2813 m/s, with a range of 1515 to 4237 m/s. According to Liu [23], the deformation modulus of the rock mass is related to the compressional wave velocity as a power function. To estimate the modulus of deformation, the borehole wave velocities of pelitic siltstone at different depths are calculated. The average wave velocity of pelitic siltstone at different depths is shown in Figure 4.

3.3. Borehole Deformation Test of the Surrounding Rock

After the borehole TV and acoustic wave test, according to the Standard for Engineering Rock Test Methods (GB/T50266-2013) and the Rock Test Procedure for Water Conservancy and Hydropower Engineering (SL/T264-2020), the borehole deformation test was conducted in the test range. A total of 42 deformation tests were carried out along the surrounding strata of the working shaft. The equipment used for the borehole deformation test is the Changjiang Academy of Sciences' CJBE91-I-type borehole elastic mode instrument. It is mainly composed of a pressurization system and a displacement testing system. In the test, two stiff pressure plates are pushed by four internal pistons to apply symmetrical strip stress to the borehole wall rock. The radial deformation of the borehole wall rock during loading is measured using displacement transducers installed in the pressure plates.

The deformation displacement under various pressures is obtained in the test. The deformation or elasticity modulus (GPa) of the rock at the test site is determined using the following formula:

$$E = A \cdot H \cdot D \cdot T(\nu, \beta) \cdot \frac{\Delta Q}{\Delta D} \quad (2)$$

where A is the influence coefficient of the three-dimensional problem calculated by the two-dimensional formula, H is the pressure correction factor, D is the diameter of the borehole (mm), ΔQ is the pressure (MPa), ΔD is the deformation increment (mm), $T(\nu, \beta)$ is the coefficient related to the size of the circumference and Poisson's ratio of rock mass when the bearing plate contacts the hole wall.

The deformation modulus of the rock mass obtained from the borehole deformation and the pressure plate test are compared. The deformation modulus is more suitable for the project and the value is selected. The shear modulus for the engineering pressure on the test pressure-deformation curve corresponds to the deformation modulus. The tangent modulus for the engineering pressure on the rock borehole deformation test parameters corresponds to the elastic modulus. The NS-ZK-6 pressure-deformation curve is shown in Figure 5. The average values of the deformation and elastic modulus vary with depth and are shown in Figure 6. The results of the borehole deformation test can be used to convert the deformation and elastic modulus of six points of the surrounding rock at various depths. An analysis of the results of six borehole elastic deformation tests revealed that the rock in the working well has a deformation modulus from 0.4 GPa to 9.4 GPa, with an average value of 4.6 GPa. The elastic modulus ranges from 0.8 GPa to 11.3 GPa with an average value of 5.7 GPa. Figure 6 illustrates the overall depth dependence of the elastic and deformation modulus of the rock surrounding. The wave velocity of pelitic siltstone is related to porosity. High crustal stress can reduce rock porosity. So, the porosity decreases with the increase in depth, and the wave velocity increases with the increase in depth. Therefore, the modulus generally increases with the depth. Within the depth of 33 m (corresponding to the elevation above about 30 m), the deformation modulus of pelitic siltstone ranges from 0.4 to 2.3 GPa, while the deformation modulus below the elevation of about -30 m ranges from 3 to 9.4 GPa.

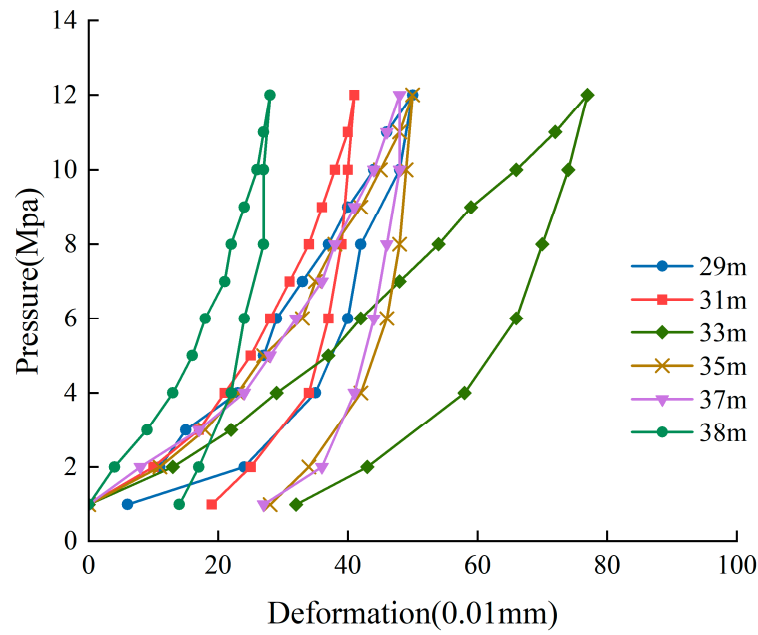


Figure 5. NS-ZK-6 borehole pressure deformation curve.

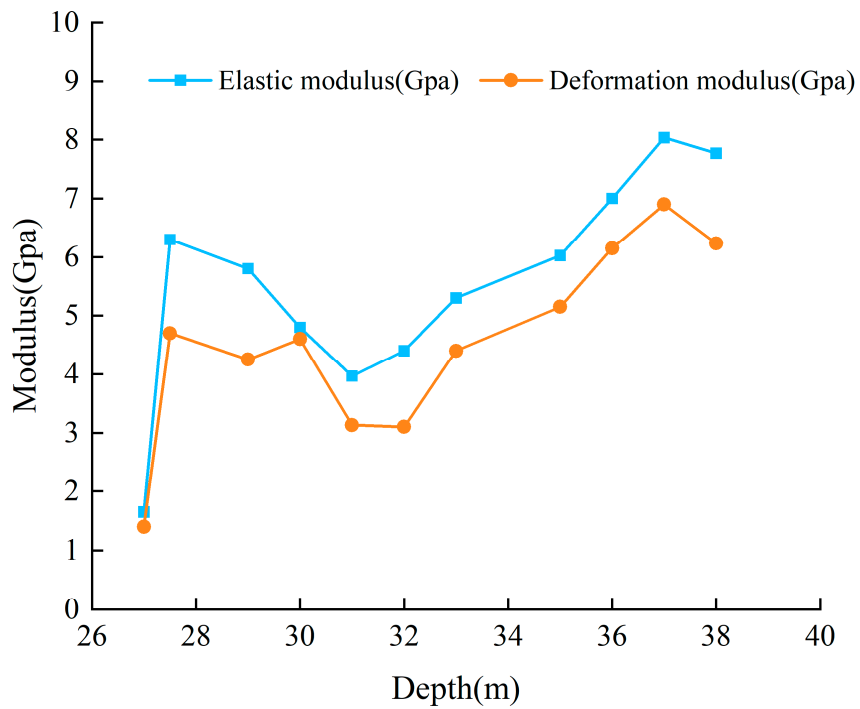


Figure 6. Variation of the average modulus with the depth.

3.4. Comparative Analysis of In Situ Test Data

3.4.1. Comparative Analysis of Borehole TV Integration

The field pressure plate test location, borehole deformation method test location, and acoustic test data are merged into the borehole TV map for comparison and additional analysis. The green line shows the borehole deformation technique test result and test site, while the red line shows the acoustic test result. After the TV results of six boreholes, it was found that four of them had deformation tests of less than 2 GPa, as shown in Figure 7.

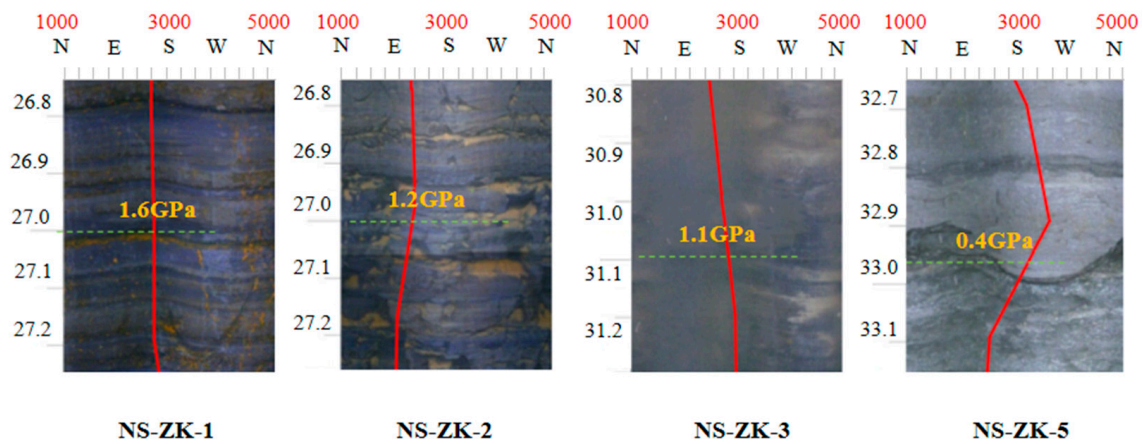


Figure 7. Borehole TV integration comparison.

NS-ZK-1 and NS-ZK-2 are readily apparent to be a part of the stratified interlayer at this position. NS-ZK-5 represents the intersection of lithologies, the borehole deformation is minimal. NS-ZK-3 depicts that there is no crack through the TV, that is, the integrity of rock mass is good. The elevation is compatible with the results of the bearing plate test (30.9 m). Through borehole TV integration, the overall situation of the rock mass can be seen directly.

3.4.2. Comparative Analysis of Deformation Modulus

The comparison results of the borehole deformation method and pressure plate test at different depths are shown in Figure 8. The results of the borehole deformation method are similar to the load plate test results. The average value of the deformation modulus is 4.71 GPa in the pressure plate test. The average value of the deformation modulus measured by the drilling method near the same elevation (borehole depth is 30.9 m) of the pressure plate test point is about 4.6 GPa. This result indicates that the borehole deformation method and load plate test can be used to confirm each other. It further demonstrates the reliability of the deformation modulus obtained by the borehole deformation method.

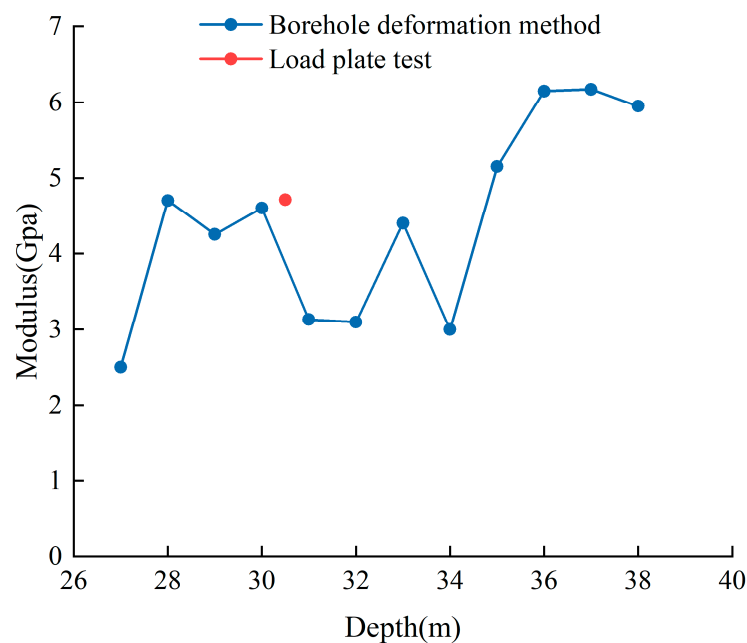


Figure 8. Comparison between borehole deformation method and pressure plate test.

According to Liu [23], it is known that the deformation modulus of the rock mass is related to the compressional wave velocity as a power function. The data measured in the field are fitted to the power function, as shown in Figure 9.

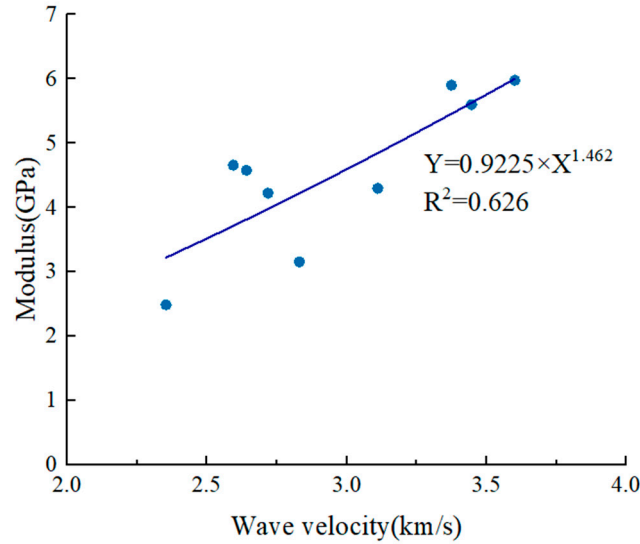


Figure 9. Relationship between modulus and wave velocity.

The following is the fitted correlation between the longitudinal wave velocity of the acoustic wave in a single hole of the pelitic siltstone and the deformation modulus of the pelitic siltstone caused by the drilling method:

$$E_s = 0.9225V_p^{1.462} \tag{3}$$

where E_s is the rock mass deformation modulus (GPa), V_p is the velocity of the single-hole acoustic p-wave in a rock mass (km/s).

The deformation modulus is derived by fitting the formula based on the results of longitudinal wave velocity tests at different borehole depths. The comparison with the deformation modulus measured by the drilling method is shown in Figure 10.

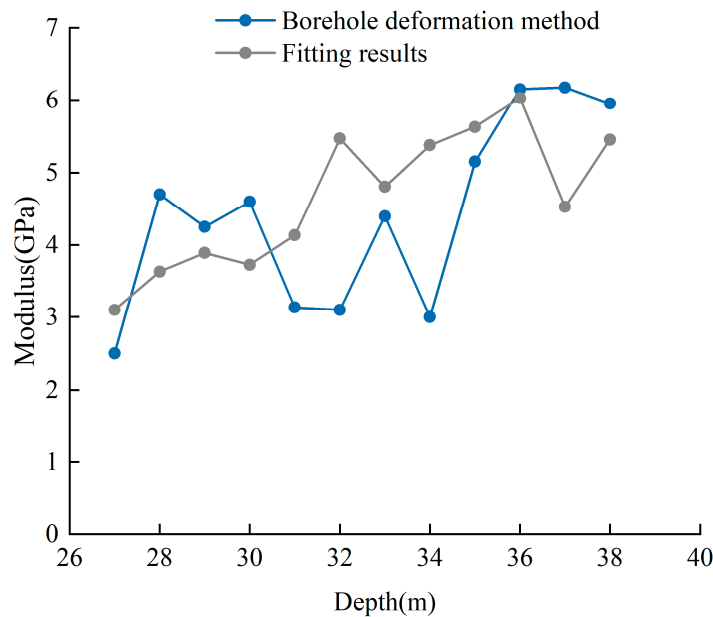


Figure 10. Comparison of fitting results and borehole deformation method.

The fitting results are similar to some extent. Combined with the wave velocity test, the average value of the deformation modulus for the weakly weathered pelitic siltstone can be computed to be substantially over 1.58 GPa.

3.4.3. Estimation of Lithologic Deformation Modulus

Based on the wave velocity test of pelitic siltstone with different stratigraphic lithologies and weathering degrees, the deformation modulus was estimated using the fitting formula. This provides a parametric basis for the numerical simulations. The deformation modulus of the pelitic siltstone in each formation is shown in Table 2.

Table 2. Estimation of deformation modulus of pelitic siltstone in different strata.

Strata Age	Lithology	Weathering Degree	P-Wave Velocity (m/s)		Deformation Modulus (GPa)		
			Range	Mean	Lower Limit	Upper Limit	Mean
Tertiary lower system Xinzhuang village group	Pelitic siltstone	Total	2008–3145	2368	2.56	4.93	3.25
		Strong	2433–3745	3288	3.38	6.36	5.26
		Weak	3175–4274	3886	4.99	7.71	6.71
Lower Cretaceous Baizushan Formation	Pelitic siltstone	Strong	2315–3745	3137	3.15	6.36	4.91

4. Combined Stress Analysis of Composite Lining

4.1. Model Establishment and Parameter Determination

The numerical tunnel model was established by ABAQUS 6.14 software. The specific dimensions of the model are shown in Figure 11. The lining is double layered. The pipe piece sheet is made of C55 concrete. The reinforced concrete lining is made of C35 concrete and HRB400 reinforcement. All these materials use the linear elastic model, and the rock mass uses the elastic-plastic model based on the Mohr–Columba (M–C) principle. The C3D8P linear hexahedral unit represents the geotechnical layer, the shield tube sheet, and the lining concrete. The T3D2 3D truss unit is used to simulate the reinforcement. The total number of units is 25,730, and the number of nodes is 31,565. The load takes into account the gravitational field, and introducing the radial load inside the tunnel, simulates the internal water pressure. The top surface of the model is free. The left and right sides apply a head pressure that changes along the gravity gradient. The bottom surface is entirely fixed. The sides are restrained from normal deformation while vertical deformation is permitted. The physical and mechanical properties of the model are shown in Table 3.

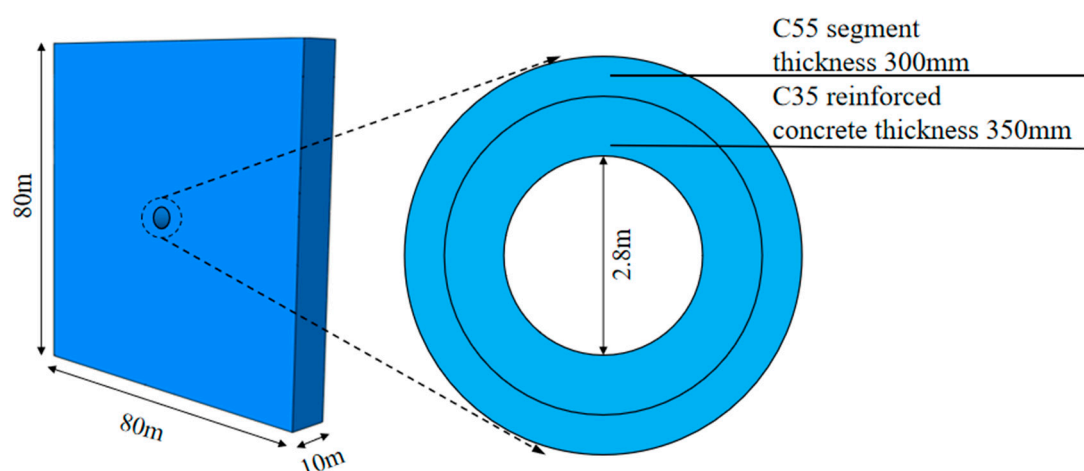


Figure 11. Overview of numerical simulation.

Table 3. Physical and mechanical parameters.

Soil Layer Name	Natural Gravity γ (kN/m ³)	Cohesion c (kPa)	Internal Friction Angle ϕ (°)	Elastic Modulus E (MPa)	Poisson Ratio μ
Artificial fill	17.5	8	11	10.74	0.4
Sludge	16.7	4	6	8.55	0.4
Sludge, muddy clay	17.3	6	7	10.35	0.3
Medium coarse sand	18	0	32	80	0.3
Gravelly sand					
Weakly weathered pelitic siltstone	20	80	26	2090	0.2
C55 concrete	25	/	/	35,500	0.166
C35 concrete	25	/	/	31,500	0.2

4.2. Setting of the Working Conditions

The porosity and permeability coefficients are frequently considered constant values in conventional rock seepage studies. In actual engineering, however, the seepage and stress fields constantly interact, changing the permeability and porosity of the material. To implement the indirect coupling study of the permeability coefficient and porosity fluctuation with the volumetric strain as the field variable, this simulation was developed secondary using ABAQUS. For the three stages of analysis, the before operation, long-term operation (5 a), and drainage maintenance were set. The dynamic evolution features of the permeability coefficient and porosity were also taken into consideration.

4.3. Simulation Results and Discussion

4.3.1. Lining Stress Analysis

The inner and outer sides of the top of the diversion tunnel lining are under tension with increasing water passage duration, as shown in Figure 12 and Table 4. The highest primary stress on the inner side steadily increased from 3.468 MPa to 5.356 MPa. The inner and outer sides of the lining waist are compressed, and the change on both sides is more symmetrical. Tremendous primary stress on the inner side rises from a compressive stress of -0.376 MPa to -1.035 MPa. The bottom of the liner was under tension on both its inner and exterior sides. The inner side experienced a rise in maximum primary stress from 3.539 MPa to 5.407 MPa. To avoid significant open fractures in the concrete lining under tension when both the top and bottom of the lining are subject to tensile stress, reinforcing can be added to the inside and outside of the lining. The inner side of the top and bottom of the lining needs special attention during the long-term operation of the diversion tunnel since there is an increase in tensile stress. It is prone to tensile cracking.

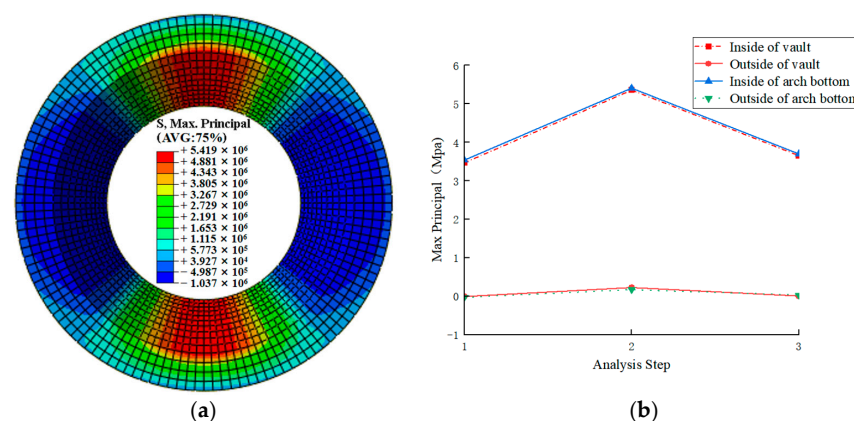


Figure 12. Stress characteristics of the lining. (a) Maximum principal stress of the lining. (b) Value of tensile part of the lining.

Table 4. Maximum principal stress of the lining.

Location	Before Operation (Mpa)	Long-Term Operation (Mpa)	Drainage Maintenance (Mpa)
Arch crown (inside/outside)	(3.468/−0.010)	(5.356/0.224)	(3.652/0.047)
Arch waist (inside/outside)	(−0.376/−0.548)	(−1.035/−0.347)	(−0.314/−0.468)
Base plate (inside/outside)	(3.539/−0.030)	(5.407/0.171)	(3.698/0.027)

4.3.2. Pipe Piece Stress Analysis

The top of the pipe piece in the diversion tunnel is subject to tension on the inside and compression on the outside as water passage time increases, as shown in Table 5 and Figure 13. The maximum principal (tensile) stress on the inside gradually increased from 0.167 Mpa to 0.572 Mpa. The pipe piece’s ring arch waist’s stress changes are also more evenly distributed on both sides. The inner and outer sides of the waist experience compression and tension, respectively. The highest principal stress on the outer side raised from 0.730 Mpa to 1.953 Mpa. The maximum primary stress on the inside of the pipe piece increased from 0.143 Mpa to 0.529 Mpa under tension on the inside and compression on the outside. The outer edge of the tube sheet waist needs special care during long-term diversion tunnel operation since this area experiences increased tensile stress and is vulnerable to tensile cracking. The pipe piece can share the internal water pressure when the liner is subjected to internal water pressure, and the stresses of the pipe piece and liner tend to be uniform under the condition of sharing the stress. This causes the maximum primary stress at the pipe piece’s waist.

Table 5. Maximum principal stress of the pipe piece.

Location	Before Operation (Mpa)	Long-Term Operation (Mpa)	Drainage Maintenance (Mpa)
Arch crown (inside/outside)	(0.167/−0.534)	(0.572/−0.612)	(0.239/−0.481)
Arch waist (inside/outside)	(−0.569/0.730)	(−0.329/1.953)	(−0.525/0.863)
Base plate (inside/outside)	(0.143/−0.582)	(0.529/−0.647)	(0.213/−0.535)

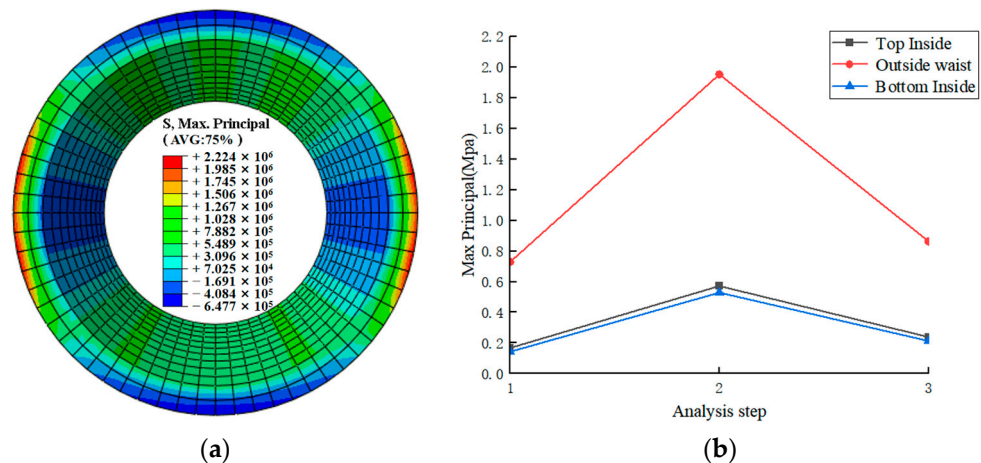


Figure 13. Stress characteristics of the segments. (a) Maximum principal stress of the segment. (b) Value of tensile part of the segment.

5. Conclusions

In this paper, the deformation characteristics of the pelitic siltstone in the Nansha Branch diversion tunnel were obtained through in situ tests. The combined stress distribution of composite lining is analyzed based on the test results and numerical method. Some conclusions are obtained as follows:

- (1) In the pressure plate test, the deformation modulus obtained by the secant and fitting method is close. The average deformation modulus of the fitting method under the water conveyance pressure of the engineering design is 4.71 GPa. The deformation modulus of 4.6 GPa is consistent with the average value measured by the borehole deformation method at the same elevation. This shows that the deformation modulus obtained by the borehole deformation method is reliable.
- (2) The horizontal bedding of the surrounding rock is developed and the integrity of the surrounding rock in the local hole section is poor according to the borehole television. The number of steep dip fractures is limited, but the width is large and there is a corrosion phenomenon. The deformation modulus of surrounding rock at the location of the diversion tunnel measured by the borehole deformation method is 0.4 GPa~9.4 GPa. The deformation modulus and elastic modulus will increase with depth.
- (3) The deformation modulus by the borehole deformation method and wave velocity obtained is fitted, and the power function relationship is obtained. Based on the acoustic test results, the deformation modulus of pelitic siltstone with various weathering degrees is estimated by using the relationship.
- (4) In the combined stress analysis of composite lining, the reinforced concrete lining of the Nansha Branch tunnel has a maximum primary stress of 5.407 Mpa, which is found inside the top and bottom. The outside edge of the waist on both sides of the pipe piece has the highest primary stress of 1.953 Mpa in tension.

Author Contributions: Conceptualization, Y.J.; methodology, Y.J.; software, Y.J.; validation, Y.H.; investigation, G.Y.; data curation, Y.H.; writing—original draft preparation, W.W.; writing—review and editing, W.W.; project administration, J.Y. All authors have read and agreed to the published version of the manuscript.

Funding: We thank the National Natural Science Foundation of China for the support of this research (52078143) and the Guangdong Provincial Science and Technology Program (2019B020208003).

Institutional Review Board Statement: Not applicable.

Informed Consent Statement: Not applicable.

Data Availability Statement: Details on all data supporting the reported results can be obtained in Tables 1–5 and Figures 3–13 in this original manuscript.

Acknowledgments: We thank the Guangdong Research Institute of Water Resources and Hydropower for providing test materials and fields for the study.

Conflicts of Interest: The authors declare no conflict of interest.

References

1. Pandey, P.; Singh, D. Deformation of a rock in different tensile tests. *Eng. Geol.* **1986**, *22*, 281–292. [[CrossRef](#)]
2. Ribacchi, R. Mechanical tests on pervasively jointed rock material: Insight into rock mass behaviour. *Rock Mech. Rock Eng.* **2000**, *33*, 243–266. [[CrossRef](#)]
3. Jafari, M.K.; Pellet, F.; Boulon, M.; Hosseini, K.A. Experimental study of mechanical behaviour of rock joints under cyclic loading. *Rock Mech. Rock Eng.* **2004**, *37*, 3–23. [[CrossRef](#)]
4. Lv, X. Exploring the deformation features and control techniques for surrounding rock of slate section tunnel. *Arab. J. Geosci.* **2020**, *13*, 1–6. [[CrossRef](#)]
5. Nal, E. Determination of in situ deformation modulus: New approaches for plate-loading tests. *Int. J. Rock Mech. Min. Sci.* **1997**, *34*, 897–915.
6. Han, L.; Zuo, Y.; Guo, Z.; Zhang, L.; Chen, X.; Mao, J. Mechanical properties and deformation and failure characteristics of surrounding rocks of tunnels excavated in soft rocks. *Geotech. Geol. Eng.* **2017**, *35*, 2789–2801. [[CrossRef](#)]
7. He, J.; Li, X.; Deng, X.; Zhang, S.; Qin, L. Mechanical properties and stability analysis of surrounding rock of underground cavern under various stress loading paths. *IOP Conf. Ser. Earth Environ. Sci.* **2021**, *861*, 042012. [[CrossRef](#)]
8. Meng, Q.-B.; Liu, J.-F.; Ren, L.; Pu, H.; Chen, Y.-L. Experimental study on rock strength and deformation characteristics under triaxial cyclic loading and unloading conditions. *Rock Mech. Rock Eng.* **2021**, *54*, 777–797. [[CrossRef](#)]

9. Meng, Q.-B.; Liu, J.-F.; Xie, L.-X.; Pu, H.; Yang, Y.-G.; Huang, B.-X.; Qian, W. Experimental mechanical strength and deformation characteristics of deep damaged–fractured rock. *Bull. Eng. Geol. Environ.* **2022**, *81*, 1–27. [[CrossRef](#)]
10. Sabitova, A.; Yarushina, V.M.; Stanchits, S.; Stukachev, V.; Khakimova, L.; Myasnikov, A. Experimental compaction and dilation of porous rocks during triaxial creep and stress relaxation. *Rock Mech. Rock Eng.* **2021**, *54*, 5781–5805. [[CrossRef](#)]
11. Vaneghi, R.G.; Thoeni, K.; Dyskin, A.V.; Sharifzadeh, M.; Sarmadivaleh, M. Fatigue damage response of typical crystalline and granular rocks to uniaxial cyclic compression. *Int. J. Fatigue* **2020**, *138*, 105667. [[CrossRef](#)]
12. Zhou, X.; Song, H.; Qian, Q. Zonal disintegration of deep crack-weakened rock masses: A non-Euclidean model. *Theor. Appl. Fract. Mech.* **2011**, *55*, 227–236. [[CrossRef](#)]
13. Cai, M.; Horii, H. A constitutive model of highly jointed rock masses. *Mech. Mater.* **1992**, *13*, 217–246. [[CrossRef](#)]
14. Singh, V.K.; Chung, S.G. Determination of deformation modulus for lower sands in nakdong river delta. *Mar. Georesources Geotechnol.* **2013**, *31*, 290–307. [[CrossRef](#)]
15. Hua, D.; Jiang, Q.; Liu, R.; Gao, Y.; Yu, M. Rock mass deformation modulus estimation models based on in situ tests. *Rock Mech. Rock Eng.* **2021**, *54*, 5683–5702. [[CrossRef](#)]
16. Radovanović, S.; Ranković, V.; Anđelković, V.; Divac, D.; Milivojević, N. Development of new models for the estimation of deformation moduli in rock masses based on in situ measurements. *Bull. Eng. Geol. Environ.* **2018**, *77*, 1191–1202. [[CrossRef](#)]
17. Asem, P. Prediction of unconfined compressive strength and deformation modulus of weak argillaceous rocks based on the standard penetration test. *Int. J. Rock Mech. Min. Sci.* **2020**, *133*, 104397. [[CrossRef](#)]
18. El Naggar, H.; Hinchberger, S.D.; Lo, K.Y. A closed-form solution for composite tunnel linings in a homogeneous infinite isotropic elastic medium. *Can. Geotech. J.* **2008**, *45*, 266–287. [[CrossRef](#)]
19. Mason, D.P.; Abelman, H. Support provided to rock excavations by a system of two liners. *Int. J. Rock Mech. Min. Sci.* **2009**, *46*, 1197–1205. [[CrossRef](#)]
20. Li, F.; Chang, N.; Wang, J.; Feng, T.; Li, C. Research on the algorithm for composite lining of deep buried water conveyance tunnel. *Adv. Civ. Eng.* **2021**, *2021*, 6686360. [[CrossRef](#)]
21. Gu, S.; He, H.; Huang, R. Stress-Strain Calculation Method of Composite Lining considering the Creep Characteristics of Tunnel Surrounding Rock. *Adv. Civ. Eng.* **2021**, *2021*, 7521435. [[CrossRef](#)]
22. Cao, R.; Wang, Y.; Zheng, L.; Zhao, Y. Influencing factors of lining crack width in hydraulic tunnels under high internal water pressure. *IOP Conf. Ser. Earth Environ. Sci.* **2020**, *570*, 052037. [[CrossRef](#)]
23. Liu, J.; Jiang, Q.; Chen, T.; Yan, S.; Ying, J.; Xiong, X.; Zheng, H. Bayesian Estimation for Probability Distribution of Rock's Elastic Modulus Based on Compression Wave Velocity and Deformation Warning for Large Underground Cavern. *Rock Mech. Rock Eng.* **2022**, *55*, 3749–3767. [[CrossRef](#)]

Disclaimer/Publisher's Note: The statements, opinions and data contained in all publications are solely those of the individual author(s) and contributor(s) and not of MDPI and/or the editor(s). MDPI and/or the editor(s) disclaim responsibility for any injury to people or property resulting from any ideas, methods, instructions or products referred to in the content.